

Theory of superconductivity in a three-orbital model of Sr_2RuO_4

Q. H. Wang¹, C. Platt², Y. Yang¹, C. Honerkamp^{3,4}, F. C. Zhang^{5,6}, W. Hanke², T. M. Rice^{5,7}, and R. Thomale^{2,8}

¹National Laboratory of Solid State Microstructures, Nanjing University, Nanjing, 210093, China

²Theoretical Physics, University of Würzburg, D-97074 Würzburg, Germany

³Institute for Theoretical Solid State Physics, RWTH Aachen University, D-52056 Aachen, Germany

⁴JARA - FIT Fundamentals of Future Information Technology, Germany

⁵Department of Physics, and Center of Theoretical and Computational Physics,
The University of Hong Kong, Hong Kong, China

⁶Department of Physics, Zhejiang University, Hangzhou, China

⁷Institute for Theoretical Physics, ETH Zurich, CH-8093 Zürich, Switzerland and

⁸Institut de théorie des phénomènes physiques, École Polytechnique Fédérale de Lausanne, CH-1015 Lausanne, Switzerland

(Dated: July 22, 2013)

In conventional and high transition temperature copper oxide and iron pnictide superconductors, the Cooper pairs all have even parity. As a rare exception, Sr_2RuO_4 is the first prime candidate for topological chiral p -wave superconductivity, which has time-reversal breaking odd-parity Cooper pairs known to exist before only in the neutral superfluid ^3He . However, there are several key unresolved issues hampering the microscopic description of the unconventional superconductivity. Spin fluctuations at both large and small wavevectors are present in experiments, but how they arise and drive superconductivity is not yet clear. Spontaneous edge current is expected but not observed conclusively. Specific experiments point to highly band- and/or momentum-dependent energy gaps for quasiparticle excitations in the superconducting state. Here, by comprehensive functional renormalization group calculations with all relevant bands, we disentangle the various competing possibilities. In particular we show the small wavevector spin fluctuations, driven by a single two-dimensional band, trigger p -wave superconductivity with quasi-nodal energy gaps.

PACS numbers: 74.20.-z, 74.20.Rp, 71.27.+a

Very soon after the discovery of superconductivity in Sr_2RuO_4 [1], it was proposed that the superconducting (SC) pairing is of unconventional nature [2, 3]. Later experiments have provided evidence that the Cooper pair in the SC state is of odd parity [4] with total spin equal to one [5]. Further evidence indicates the superconductivity to be chiral, breaking time reversal symmetry [6, 7]. Sr_2RuO_4 is thus the first prime candidate for a chiral p -wave superconductor [8–11], an interesting analogue of the neutral superfluid ^3He . It has recently received great interest as by suitable manipulations it may support zero energy Majorana bound states in vortices [12], the building block for topological quantum computing [13]. However, there are a number of outstanding issues associated with the chiral p -wave superconductivity in Sr_2RuO_4 . First, p -wave spin triplet pairing is expected to be associated with spin fluctuations at small wavevector. However, the spin density wave (SDW) fluctuation observed in Sr_2RuO_4 is dominated by a large wavevector at higher temperatures and coexist with a feature at small wavevector at lower temperatures. [14] A resolution of this puzzle is vital to understand the superconductivity. Second, one would expect a spontaneous electric current at the edge of the RuO_2 layers as a result of the chiral SC state. The edge current, however, has not been observed conclusively in experiments. [15] One possible reason is the edge current is very fragile and difficult to establish against disorders. Another possibility is a topological cancellation from hole-like and electron-like bands, [16] posing a ques-

tion as whether the SC state is topologically nontrivial at all. Third, the specific measurement reveals abundance of low energy quasiparticle excitations below the transition temperature. [17] This would point to multiple gaps of very different magnitudes and/or deep minima in strongly momentum dependent gap functions. Previous theories treat either the two-dimensional (2D) γ -band derived from the xy orbital, [18–21] or the quasi-one-dimensional (1D) α and β bands derived from the xz and yz orbitals. [16, 22] However, the evolution of wavevectors of the spin fluctuations is beyond such models, and in fact can only be accounted for by a complete three-band model. This in turn dictates the properties of the SC state mentioned above. *A microscopic theory for ruthenate superconductivity should explain both SDW and SC fluctuations at different energy or temperature scales.* In this paper, we apply the functional renormalization group theory (FRG) [20, 23] to study a 3-band Hubbard model including both the 2D- γ and the quasi-1D (α, β) Fermi sheets as suggested by first-principle calculations and angle-resolved photoemission (ARPES) experiments. [9, 24] The FRG is particularly promising to address the multi-scale energy issues in ruthenates. In recent years the FRG has been expanded to treat 2D multi-orbital systems such as the iron pnictides and selenides [25–27] and candidate models of topological superconductors with or without time-reversal symmetry [28–32]. In addition to addressing the pairing symmetry and energy scale, FRG gives information on the relative strength and wavevector of competing orders in the particle-hole chan-

nels. Our results show that the SDW fluctuations are driven mainly by two 1D bands at the large wavevector and by the 2D band at the small wavevector, successively as the energy scale is lowered. The latter triggers at an even lower energy scale p -wave superconductivity, which is dominated by the 2D band and has a highly anisotropic gap and deep minima near the Brillouin zone boundary. Our theory predicts chiral edge modes and thus edge current. However, the large gap anisotropy indicates the fragility of the chiral edge modes against perturbations such as disorder, rendering the detection of edge current hard to accomplish. Our prediction on the strong SDW fluctuations at a small wavevector at low temperatures can be tested in further neutron scattering experiment, and the prediction on the strongly anisotropic gap function in momentum space should be tested in ARPES with high resolution at extremely low temperatures.

The model we consider is described by the Hamiltonian

$$\begin{aligned}
 H = & \sum_{\mathbf{k}, \sigma} \psi_{\mathbf{k}a\sigma}^\dagger \epsilon_{\mathbf{k}}^{ab} \psi_{\mathbf{k}b\sigma} + U \sum_{i,a} n_{ia\uparrow} n_{ia\downarrow} + U' \sum_{i,a>b} n_{ia} n_{ib} \\
 & + J \sum_{i,a>b, \sigma, \sigma'} \psi_{ia\sigma}^\dagger \psi_{ib\sigma} \psi_{ib\sigma'}^\dagger \psi_{ia\sigma'} \\
 & + J' \sum_{i,a \neq b} \psi_{ia\uparrow}^\dagger \psi_{ia\downarrow}^\dagger \psi_{ib\downarrow} \psi_{ib\uparrow}.
 \end{aligned} \quad (1)$$

Here, \mathbf{k} denotes the momentum, σ the spin, i the lattice site, and a and b the orbital labels, with $\psi_{a=1,2,3}$ annihilating an electron in d_{xz} , d_{yz} and d_{xy} orbitals, respectively. The local interaction parameters include intraorbital (U), interorbital (U'), Hund's (J), and pair hopping (J'). The matrix dispersion function $\epsilon_{\mathbf{k}}^{ab}$ has the following nonzero elements: $\epsilon_{\mathbf{k}}^{11} = -2t_1 \cos k_x - \mu$, $\epsilon_{\mathbf{k}}^{22} = -2t_1 \cos k_y - \mu$, $\epsilon_{\mathbf{k}}^{12/21} = -4t_2 \sin k_x \sin k_y$, and $\epsilon_{\mathbf{k}}^{33} = -2t'_1 (\cos k_x + \cos k_y) - 4t'_2 \cos k_x \cos k_y + \Delta - \mu$, where in dimensionless units, $t_1 = 1$, $t_2 = 0.1$, $t'_1 = 0.8$, $t'_2 = 0.35$, $\Delta = -0.2$ is the crystal field splitting, and $\mu = 1.1$ is the chemical potential. This set of parameters produces the band structure shown in Fig. 1a. The inset shows the Fermi surface, which resembles closely what is observed experimentally [9, 24]. The corresponding normal state density of states is shown in Fig. 1b. There are van Hove points at the X points on the γ -band close to the Fermi level, while the band edge anomalies of the α and β bands are far from the Fermi level.

As known for such a system with partial nesting and van Hove singularities near the Fermi level, there will be various competing and mutually interacting collective fluctuations in density-wave and pairing channels. This physics can be investigated appropriately by FRG. It provides coupled flow of wavevector resolved effective interactions in all particle-particle and particle-hole channels versus a running energy scale Λ . We use the singular-mode FRG (SMFRG) [27, 29, 33] to gain benefit of resolving the interactions throughout the Brillouine zone in terms of form factors, and use the multi-patch

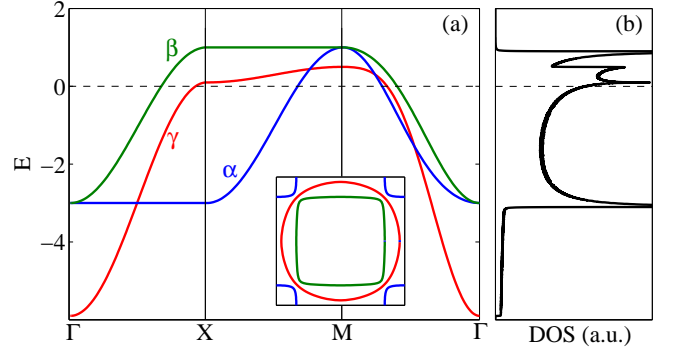


FIG. 1. Band structure of the Sr_2RuO_4 model. (a) Dispersion along high symmetry cuts. (Inset: Fermi surface structure with two quasi 1D bands and one 2D band.) (b) Density of states resulting from (a).

FRG [20, 23] to check, with increased angular resolution, that no important form factors have been left out. From the combination the dominant ordering tendencies can be most suitably addressed. See Supplementary Materials for technical details. In both schemes, the effective interaction at a given scale can always be decomposed as,

$$V^{ab;cd}(\mathbf{k}, \mathbf{k}', \mathbf{q}) \rightarrow \sum_m S_m(\mathbf{q}) \phi_m^{ab}(\mathbf{k}, \mathbf{q}) [\phi_m^{cd}(\mathbf{k}', \mathbf{q})]^*, \quad (2)$$

either in the SC, spin or charge channels. Here a, b, c, d are orbital or band labels, \mathbf{q} is the associated collective wavevector, and \mathbf{k} (or \mathbf{k}') is an internal momentum of the fermion bilinears $\psi_{\mathbf{k}+\mathbf{q},a}^\dagger \psi_{-\mathbf{k},b}$ and $\psi_{\mathbf{k}+\mathbf{q},a}^\dagger \psi_{\mathbf{k},b}$ in the particle-particle and particle-hole channels, respectively. (The Cooper instability occurs at $\mathbf{q} = 0$ in the particle-particle channel). The most attractive or fastest growing one of the eigenvalues $S_m(\mathbf{q})$ represents the dominant ordering tendency in the respective channel. The divergence energy scale is an upper estimate for the ordering temperature.

In Fig. 2 we show the SMFRG flow of the leading eigenvalues in the (a) spin and (b) SC channel, for bare interactions $(U, U', J, J') = (3.2, 1.3, 0.3, 0.3)$. In (a), changes in the dominant wavevector of the spin interaction are marked by arrows. At high scales, the spin channel dominates over the SC channel. The dominant spin-fluctuation wavevector evolves from $\mathbf{q} = (1, 1)\pi$ to $\mathbf{q} \sim \mathbf{q}_1 = (0.625, 0.625)\pi$ as Λ decreases. For $\Lambda < 5 \times 10^{-3}$, a further level crossing to $\mathbf{q} \sim \mathbf{q}_2 = (0.188, 0.188)\pi$ occurs. We checked the form factors $\phi_m^{ab}(\mathbf{k}, \mathbf{q})$ to find that the \mathbf{q}_2 -feature comes dominantly from the γ -band, while the α and β bands mainly contribute to the \mathbf{q}_1 -feature. The spin response at \mathbf{q}_2 is due to the proximity to the van Hove singularity in the γ -band mentioned previously. This spots an effect that can not be detected in an analysis for vanishingly small interactions [16], as a finite interaction scale is needed for the proximate van Hove points to come into play. The evolution of the spin-fluctuation peak from larger to small \mathbf{q} with decreasing energy scale

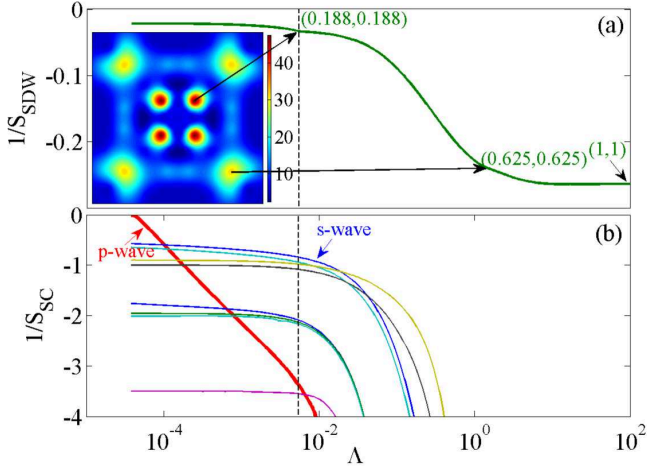


FIG. 2. (a) FRG flow of the leading eigenvalue $S_{SDW}(\mathbf{q})$ in the spin channel. The inset shows the \mathbf{q} -map at the instability scale. (b) Leading pairing eigenvalues $S_{SC}(\mathbf{q} = 0)$. The thick line denotes the two eventually diverging p -wave pairing modes. Arrows indicate level crossings associated with the evolution of the \mathbf{q}/π in the spin channel in (a) and the pairing symmetries in (b). The vertical dashed line highlights the correlation between the emergence of small- \mathbf{q} -spin feature and the p -wave pairing tendency.

is in good qualitative agreement with neutron scattering experiments [14] where a similar change is observed as a function of temperature. The charge channel (not shown) is screened down in the flow and only re-enhanced weakly as Λ decreases. At lowest scales, both spin and charge channels saturate due to imperfect nesting.

In the inset of Fig. 2, we plot the leading spin-channel eigenvalues $S_{SDW}(\mathbf{q})$ versus \mathbf{q} at the final stage of the RG flow. We see that the interaction in the spin channel peaks at \mathbf{q}_2 , but the amplitude at \mathbf{q}_1 is also sizable. In both cases, the spin bilinears correspond to onsite spins. The attractive pairing interaction is induced at intermediate scales via the spin channel. As the dominant spin fluctuation vector changes during the flow, the dominant pairing fluctuations also undergo changes as a function of Λ . In Fig. 2b, we show the 10 leading attractive eigenvalues of the pairing channel. At low scales, the strongest growing eigenvalue belongs to a p -wave mode which is two-fold degenerate due to the underlying C_{4v} symmetry. By comparing the flow in the spin channel in (a), we see that this pairing mode is already seeded and enhanced as the \mathbf{q}_2 -feature shows up (the correlation is shown by the vertical dashed line), supporting the interpretation that close-to-ferromagnetic spin fluctuations drive triplet p -wave pairing in this case. The final portion of the SC flow is log-linear in Λ , consistent with the fact that the spin and charge channels saturate and decouple from the SC channel in the lowest energy range.

We now analyze the detailed pairing function of the p -wave state. Fig. 3a shows the form factors of the two

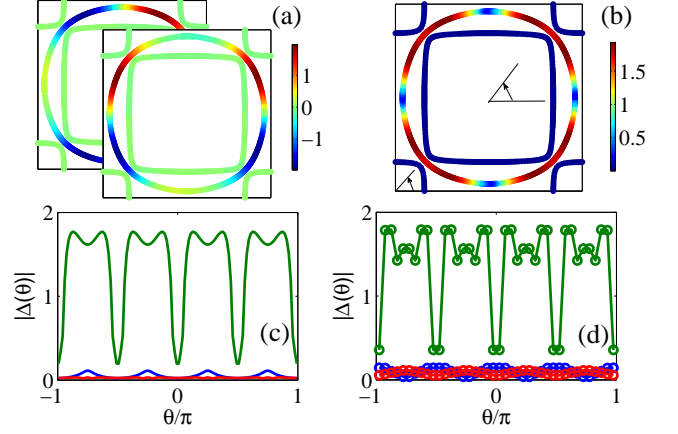


FIG. 3. The gap structure (not to scale). (a) Leading p -wave form factors on the Fermi surfaces. (b) $p + ip'$ gap amplitude $|\Delta(\mathbf{k})|$ on the Fermi surfaces. (c) The Fermi angle θ dependence of $|\Delta(\theta)|$ for the pockets α (blue), β (red) and γ (green) as obtained by SMFRG. θ is defined according to the arrows in (b). The amplitudes on α and β sheets are enlarged for better visibility. (d) Same plot as (c) obtained by multi-patch FRG without rescaling of the α and β sheet.

degenerate p -wave functions. For the Fermiology and interaction regime considered, the gap function in SMFRG turns out to be much smaller on the α and β bands than on the γ -band, in general agreement with multipatch FRG. On the γ band, the degenerate gap form factors from the SMFRG can be written approximately as $p_{\mathbf{k}} = p_1 \sin k_x + p_2 \cos k_y \sin k_x$ and $p'_{\mathbf{k}} = p_1 \sin k_y + p_2 \cos k_x \sin k_y$, where $p_1/p_2 = -0.4375$. Thus, it is worth noting that pairing on the next-nearest bond is important. In the ordered state, as confirmed by a mean field calculation using the renormalized pairing interaction, the favorable state resulting from the p -wave instability is the chiral $p \pm ip'$ state, as the system maximizes condensation energy by breaking time-reversal symmetry. The gap amplitude $|\Delta(\mathbf{k})|$ in this case is shown in Fig. 3b on the Fermi surface. For better quantitative clarity, in Fig. 3c we plot the Fermi angle θ dependence of $|\Delta(\theta)|$ on the Fermi pockets α (blue), β (red) and γ (green). Since the amplitudes on the α and β pockets are very small, they are enlarged (by a factor of 20) for better visibility. Near X/Y , the γ -band gap amplitude shows deep minima. This is understood as follows. In general, p -wave pairing is stabilized by attractive (repulsive) interactions upon forward (backward) scattering. The umklapp contribution to backward scattering, however, involves only a small momentum transfer, leading to a destructive interference. In this sense, the p -wave pairing for such a Fermi surface cannot benefit from the enhanced density of states near X/Y , and correspondingly, the energy scale for it is small (we get $\sim 0.1\text{meV}$). The low critical scale is also consistent with the late emergence of the small- q spin fluctuations shown in Fig. 2a.

The depth of the gap minima is enhanced by the second nearest-neighbor pairing p_2 with opposite sign to p_1 . The deep minimum feature is likewise found in multi-patch FRG (Fig. 3d). There, the angular variation is found to be slightly stronger than for SMFRG, while the general behavior is the same. Similarly, also for the multi-patch FRG, the gap on the α and β -pockets is rather small, even below the minimum on the γ -band. While the qualitative behavior is similar to that of Ref. [21], the anisotropy and band-selectiveness of the pairing is even stronger in our infinite-order approach.

The deep gap minima on the γ -band define a small gap scale of roughly a tenth of the gap maximum. We discuss two consequences of this small energy scale: Fig. 4 shows the energy spectrum of the $p + ip'$ SC meanfield Hamiltonian on an infinite ribbon along the y -direction, with open boundary conditions along x . The energy eigenvalues are plotted versus the transverse momentum k_y . The circles denote the amplitude of the wavefunctions on one of the two edges. We see that there are subgap edge modes that are unidirectional, i.e. chiral. The gapless bands localized on either edge cross at $k_y = 0$. There are two additional energy minima of the edge states near $k_y = \pm\pi$ that appear to be connected to the large second nearest-neighbor pairing component p_2 which in turn enhances bulk gap minima. Note that the gapless chiral edge states are protected only up to the deep bulk gap minima, beyond which impurity scattering between the edge modes and the bulk continuum is allowed. The edge modes within the bulk gap minimum may be robust but such low energy Bogoliubov de Gennes quasiparticles are almost charge neutral. This severely reduces the robustness of the chiral edge current with respect to, *e.g.*, edge disorder. Experimentally the detection of the edge current is not yet conclusive.[15]

In thermodynamic quantities, the γ -band contributes significantly once the temperature is about the SC gap scale, in addition to the α - and β -bands. In particular, while there are still open questions about the role of (α, β) bands, the deep gap minima might contribute to explaining the power-law behavior in the specific heat at temperatures above the small gap scale. [21] This argument is similar in spirit to a recent discussion of possible anisotropic chiral d -wave superconductivity in sodium cobaltates [31].

Before closing we emphasize that the results for these qualitative features of the gap structure discussed so far are quite generic. (A detailed discussion of the general phase diagram of the given Fermiology beyond the specific ruthenate setting will be given elsewhere.) We obtain rather similar results for a considerable range of interactions, *e.g.*, $(U, U', J, J') = (3.3, 1.1 \pm 0.1, 0.115, 0.115)$, where the only varying aspect we find from the data is the absolute instability scale of superconductivity. A general trend we find is that the Hund's rule coupling J and pair hopping J' favor large- \mathbf{q} SDW inter-

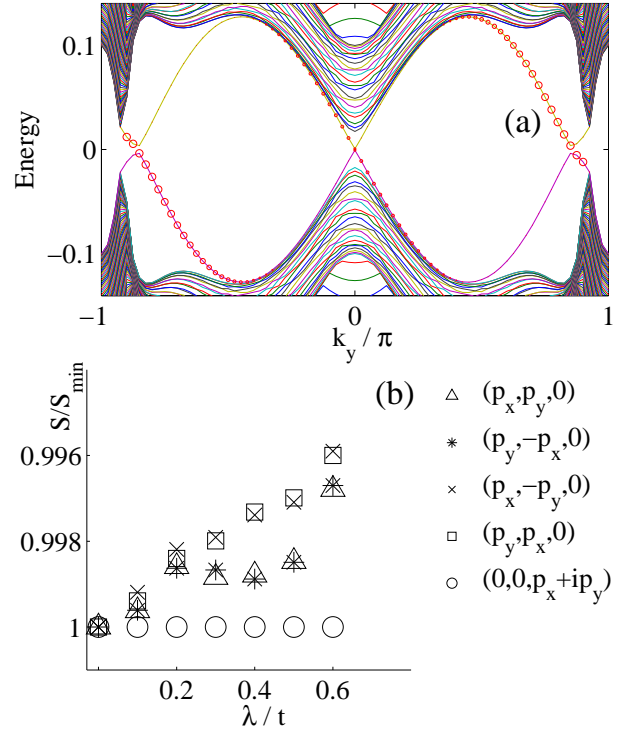


FIG. 4. (a) Energy spectrum versus the transverse momentum k_y in the $p + ip'$ SC state of a ribbon under open boundary conditions along x . Only the d_{xy} -orbitals are considered. The size of the circles denotes the wave function amplitude of the low-lying edge states integrated over two sites nearest to the respective edge. (b) Relative pairing eigenvalues versus spin-orbit coupling λ . The legend shows the five types of \mathbf{d} -vector in the triplet pairing function. S_{min} is the most attractive eigenvalue.

actions, and if sufficiently large, would destabilize the p -wave pairing. Atomic spin-orbital coupling and inter-layer hopping mixes d_{xz}/d_{yz} ($n = 1, 2$) and d_{xy} ($n = 3$) orbitals at the one-particle level, leading to inter-band proximity effect between the active and passive bands which may contribute to the pairing amplitude on the α - and β -bands [34]. (At the level of interactions, the pair hopping J' is the only coupling which would allow for a proximity effect induced by the γ -band, and the effect is weak since this coupling is initially orthogonal to the p -wave channel.) To a good approximation, such effects can be included by using the above renormalized pairing interaction at a suitable energy scale Λ_0 , and continue the flow in the pairing channel alone, since the particle-hole channel is essentially saturated and decoupled from the pairing channel at this stage. The behavior of the eigenvalues of the pairing channel as a function of spin-orbit coupling strength $\frac{i\lambda}{2}\epsilon_{abn}\sigma_{ss'}^n\psi_{\mathbf{k},a,s}^\dagger\psi_{\mathbf{k},b,s'}$ (where ϵ is the antisymmetric tensor and σ is the Pauli matrix, and repeated orbital and spin labels are implicitly summed over) is shown in Fig. 4b. This leads us to the conclusion that the most favorable triplet pairing \mathbf{d} -vector is

$\mathbf{d}_{\mathbf{k}} = (p_{\mathbf{k}} \pm ip'_{\mathbf{k}})\hat{z}$, as already found in previous works based on qualitative arguments. However, given the small splitting in the eigenvalues, an applied magnetic field could weaken the effect of spin-orbital coupling in favor of Majorana zero modes in vortices [12, 13].

To conclude, we studied the pairing mechanism in Sr_2RuO_4 within a three-orbital model by extensive FRG calculations that go beyond previous approaches for this system in that they take into account all three relevant bands and the competition between various interaction channels to arbitrary order in the bare couplings. The different FRG approaches we employ show the same trends in the dominant p -wave pairing and SDW channels: We find that the momentum \mathbf{Q} of the dominant SDW interaction evolves from $\mathbf{Q} \sim (2/3, 2/3)\pi$ at high energy scales to $\mathbf{Q} \sim (1/5, 1/5)\pi$ at low scales. The small- \mathbf{Q} SDW fluctuations drive p -wave Cooper pairing predominantly on the γ -band derived from the d_{xy} -orbital. The pairing receives contributions from first and second-nearest neighbors on the Ru square lattice. The energetically most favorable combination of a $p \pm ip'$ -gap function has deep minima in amplitude on the γ -Fermi surface near $(\pi, 0)$ and $(0, \pi)$. This makes the chiral edge modes fragile already against a moderate amount of impurities.

We thank S. A. Kivelson, J. X. Li and M. Sigrist for interesting discussions. All authors agree to the contents of the paper, and have contributed to the paper extensively. TMR, FCZ and QHW initiated the project by using SMFRG, and WH, CH and RT initiated the project by using patch fRG. QHW and YY performed SMFRG calculations, and RT and CP performed patch fRG calculations. TMR and CH contributed to the coordination of SMFRG and fRG calculations. QHW, TMR, FCZ, CH, and RT contributed to the writing. There are no financial conflicts among the authors. All correspondence should be addressed to TMR (rice@phys.ethz.ch) and/or QHW (qhwang@nju.edu.cn). This work was supported by NSFC (under grant No.10974086, No. 11274269 and No.11023002), the Ministry of Science and Technology of China (under grant No.2011CBA00108 and 2011CB922101), DFG FOR 723, 912 and SPP 1458, and by the Swiss Nationalfonds.

[1] Maeno, Y. *et al.* Superconductivity in a layered perovskite without copper. *Nature* **372**, 532-534(1994).
[2] Rice, T. M. & Sigrist, M. Sr_2RuO_4 : an electronic analogue of ^3He ?. *J. Phys. Condens. Matter* **7**(47), L643 (1995).
[3] Baskaran, G. Why is Sr_2RuO_4 not a high T_c superconductor? Electron correlation, Hund's coupling and p -wave instability. *Physica B* **224**, 490-495 (1996).
[4] Nelson, K. D. *et al* Odd-parity superconductivity in

Sr_2RuO_4 . *Science* **306**, 1151-1154 (2004).
[5] Ishida, K. *et al.* Spin-triplet superconductivity in Sr_2RuO_4 identified by O-17 Knight shift. *Nature* **396**, 658-660 (1998).
[6] Luke, G. M. *et al.* Time-reversal symmetry breaking superconductivity in Sr_2RuO_4 . *Nature* **394**, 558-561 (1998).
[7] Kapitulnik, A., Xia, J., Schemm, E., & Palevski, A. Polar Kerr effect as probe for time-reversal symmetry breaking in unconventional superconductors, *New J. Phys.* **11**, 055060 (2009).
[8] Mackenzie, A. P. & Maeno, Y. The superconductivity of Sr_2RuO_4 and the physics of spin-triplet pairing. *Rev. Mod. Phys.* **75**, 657-712 (2003).
[9] Bergemann, C. *et al.* Quasi-two-dimensional Fermi liquid properties of the unconventional superconductor Sr_2RuO_4 . *Advances in Physics* **52**, 639-725 (2003).
[10] Maeno, Y. *et al.* Evaluation of Spin-Triplet Superconductivity in Sr_2RuO_4 . *J. Phys. Soc. Jpn.* **81**, 011009 (2012).
[11] Kallin, C. Chiral p -wave order in Sr_2RuO_4 . *Rep. Prog. Phys.* **75**, 042501 (2012).
[12] Ivanov, D. A. Non-Abelian statistics of half-quantum vortices in p -wave superconductors. *Phys. Rev. Lett.* **86**, 268 (2001); Read, N. & Green, D. Paired states of fermions in two dimensions with breaking of parity and time-reversal symmetries and the fractional quantum Hall effect. *Phys. Rev. B* **61**, 10267 (2000).
[13] Nayak, C. *et al.* Non-Abelian anyons and topological quantum computation. *Rev. Mod. Phys.* **80**, 1083 (2008).
[14] Braden, M. *et al.* Inelastic neutron scattering study of magnetic excitations in Sr_2RuO_4 . *Phys. Rev. B* **66**, 064522 (2002).
[15] Kirtley, J. R., *et al.* Upper limit on spontaneous supercurrents in Sr_2RuO_4 . *Phys. Rev. B* **76**, 014526 (2007).
[16] Raghu, S., Kapitulnik, A. & Kivelson, S. A. Hidden quasi-one-dimensional superconductivity in Sr_2RuO_4 . *Phys. Rev. Lett.* **105**, 136401 (2010); Chung, S. B., Raghu, S., Kapitulnik, A. & Kivelson, S. A. Charge and spin collective modes in a quasi-one-dimensional model of Sr_2RuO_4 . *Phys. Rev. B* **86**, 064525 (2012); Raghu, S., Chung, S. B., Lederer, S. Theory of 'hidden' quasi-1D superconductivity in Sr_2RuO_4 . *arXiv: 1208.6344*.
[17] Agterberg, D. F., Rice, T. M. & Sigrist, M. Orbital Dependent Superconductivity in Sr_2RuO_4 . *Phys. Rev. Lett.* **78**, 3374-3377 (1997).
[18] Hlubina, R. Phase diagram of the weak-coupling two-dimensional $t-t'$ Hubbard model at low and intermediate electron density. *Phys. Rev. B* **59**, 9600 (1999).
[19] Nomura, T. & Yamada, K. Perturbation Theory of Spin-Triplet Superconductivity for Sr_2RuO_4 . *J. Phys. Soc. Jpn.* **69**(11), 3678-3688 (2000).
[20] Honerkamp, C. & Salmhofer, M. Magnetic and Superconducting Instabilities of the Hubbard Model at the van Hove Filling. *Phys. Rev. Lett.* **87**, 187004 (2001); Honerkamp, C. & Rice, T. M. Cuprates and Ruthenates: Similarities and Differences *J. Low Temp. Phys.* **131**, 159 (2003).
[21] Nomura T. & Yamada, K. Detailed Investigation of Gap Structure and Specific Heat in the p -wave Superconductor Sr_2RuO_4 . *J. Phys. Soc. Jpn.* **71**(2), 404-407 (2002).
[22] Huo, J., Rice, T. M. & Zhang, F. C. Spin Density Wave Fluctuations and p -wave Pairing in Sr_2RuO_4 . *Phys. Rev. Lett.* **110**, 167003 (2013).

- [23] Metzner, W. *et al.* Functional renormalization group approach to correlated fermion systems. *Rev. Mod. Phys.* **84**, 299-352 (2012).
- [24] Damascelli, A. *et al.* Fermi Surface, Surface States, and Surface Reconstruction in Sr_2RuO_4 . *Phys. Rev. Lett.* **85**, 5194 (2000).
- [25] Wang, F., Zhai, H., Ran, Y., Vishwanath, A. & Lee, D. H. Functional Renormalization-Group Study of the Pairing Symmetry and Pairing Mechanism of the FeAs-Based High-Temperature Superconductor. *Phys. Rev. Lett.* **102**, 047005 (2009).
- [26] Thomale, R., Platt, C., Hanke, W. & Bernevig, B. A. Mechanism for Explaining Differences in the Order Parameters of FeAs-Based and FeP-Based Pnictide Superconductors. *Phys. Rev. Lett.* **106**, 187003 (2011); Thomale, R. *et al.* Exotic d -Wave Superconducting State of Strongly Hole-Doped $\text{K}_x\text{Ba}_{1-x}\text{Fe}_2\text{As}_2$. *Phys. Rev. Lett.* **107**, 117001 (2011).
- [27] Xiang, Y. Y. *et al.* High-temperature superconductivity at the FeSe/SrTiO₃ interface. *Phys. Rev. B* **86**, 134508 (2012).
- [28] Kiesel, M. L. *et al.* Competing many-body instabilities and unconventional superconductivity in graphene, *Phys. Rev. B* **86**, 020507 (2012).
- [29] Wang, W. S. *et al.* Functional renormalization group and variational Monte Carlo studies of the electronic instabilities in graphene near $\frac{1}{4}$ doping. *Phys. Rev. B* **85**, 035414 (2012).
- [30] Wang, W. S., Li, Z. Z., Xiang, Y. Y. & Wang, Q. H. Competing electronic orders on kagome lattices at van Hove filling. *Phys. Rev. B* **87**, 115135 (2013).
- [31] Kiesel, M. L., Platt, C., Hanke, W., Thomale R. Anisotropic chiral $d+id$ superconductivity in $\text{Na}_x\text{CoO}_2 \cdot y\text{H}_2\text{O}$, *arXiv*:1301.5662.
- [32] Xiang, Y. Y., Wang, W. S., Wang, Q. H. & Lee, D. H. Topological superconducting phase in the vicinity of ferromagnetic phases. *Phys. Rev. B* **86**, 024523 (2012).
- [33] Husemann, C. & Salmhofer, M. Efficient parametrization of the vertex function, Ω scheme, and the t, t' Hubbard model at van Hove filling. *Phys. Rev. B* **79** 195125 (2009); Giering, K.-U. & Salmhofer, M. Self-energy flows in the two-dimensional repulsive Hubbard model. *Phys. Rev. B* **86**, 245122 (2012).
- [34] Zhitomirsky, M. E. & Rice, T. M. Interband Proximity Effect and Nodes of Superconducting Gap in Sr_2RuO_4 . *Phys. Rev. Lett.* **87**, 057001 (2001).